Optimal fluorescence excitation wavelengths for detection of squamous intra-epithelial neoplasia: results from an animal model

Lezlee Coghlan
Dept. of Veterinary Sciences, The University of Texas M.D. Anderson Cancer Center, Science Park, Bastrop, TX

Urs Utzinger, Rebekah Drezek, Douglas Heintzelman, Andres Zuluaga, Carrie Brookner and Rebecca Richards-Kortum
The Dept. of Electrical and Computer Engineering and The Biomedical Engineering Program, The University of Texas, Austin, TX
kortum@mail.utexas.edu

Irma Gimenez-Conti
Dept. of Carcinogenesis, The University of Texas M.D. Anderson Cancer Center, Science Park, Smithville, TX

Michele Follen
Dept. of Gynecologic Oncology, The University of Texas M.D. Anderson Cancer Center, Houston, TX

Abstract: Using the hamster cheek pouch carcinogenesis model, we explore which fluorescence excitation wavelengths are useful for the detection of neoplasia. 42 hamsters were treated with DMBA to induce carcinogenesis, and 20 control animals were treated only with mineral oil. Fluorescence excitation emission matrices were measured from the cheek pouches of the hamsters weekly. Results showed increased fluorescence near 350-370 nm and 410 nm excitation and decreased fluorescence near 450-470 nm excitation with neoplasia. The optimal diagnostic excitation wavelengths identified using this model - 350-370 nm excitation and 400-450 nm excitation - are similar to those identified for detection of human oral cavity neoplasia.

OCIS codes: (170.6280) Spectroscopy, fluorescence and luminescence; (170.6510) Spectroscopy, tissue diagnostics

References and Links

1. E. Sevick-Muraca and R. Richards-Kortum, "Quantitative optical spectroscopy for tissue diagnosis," Ann Rev Phys Chem **47**, 555-606 (1996).
2. G.A. Wagnieres, W.M. Star, and B.C. Wilson, "In vivo fluorescence spectroscopy and imaging for oncological applications," Photochemistry and Photobiology **68**, 603-32 (1998).
3. H. Stepp, R. Sroka, R. Baumgartner, "Fluorescence endoscopy of gastrointestinal diseases: basic principles, techniques, and clinical experience," Endoscopy **30**, 379-86 (1998).
4. S.P. Schantz, V. Kolli, H.E. Savage, G. Yu, J.P. Shah, D.E. Harris, A. Katz, R.R. Alfan, and A.G. Huvos "In vivo native cellular fluorescence and histological characteristics of head and neck cancer," Clinical Cancer Research **4**, 1177-1182 (1998).
5. A.R.Gillenwater, R. Jacob, R. Ganeshappa, B. Kemp, A.K. El-Naggar, J.L. Palmer, G. Clayman, M.F. Mitchell, and R. Richards-Kortum, "Noninvasive diagnosis of oral neoplasia based on fluorescence spectroscopy and native tissue autofluorescence," Archives of Otolaryngology – Head and Neck Surgery **124**, 1251-1258 (1998).
6. V. Kolli, H.E. Savage, T.J. Yao, and S.P. Schantz, "Native cellular fluorescence of neoplastic upper aerodigestive mucosa," Arch. Otolaryng. Head Neck Surg. **121**, 1287-92 (1995).
7. D.R. Ingrams, J.K. Dhingra, K. Roy, D.F. Perrault Jr., I.D. Bottrill, S. Kabani, E.E. Rebeiz, M.M. Pankratov, S.M. Shapshay, R. Manoharan, I. Itzkan, and M.S. Feld, "Autofluorescence characteristics of oral mucosa," Head & Neck **19**, 27-32 (1997).
8. N. Ramanujam, M. Follen-Mitchell, A. Mahadevan-Jansen, S. Thomsen, G. Staerkel, A. Malpica, T. Wright, N. Atkinson and R. Richards-Kortum, "Cervical precancer detection using multivariate statistical

#26869 - $15.00 US Received October 20, 2000; Revised December 01, 2000

algorithm based on laser-induced fluorescence spectra at multiple excitation wavelengths," Photochemistry and Photobiology **64**, 720-735 (1996).
9. A. Agrawal, U. Utzinger, C. Brookner, C. Pitris, M. F. Mitchell, R. Richards-Kortum, "Fluorescence spectroscopy of the cervix: influence of acetic acid, cervical mucus, and vaginal medications," Lasers in Surgery & Medicine, **25**, 237-49 (1999).
10. K. Schomacker, J. Frisoli, C. Compton, T. Flotte, J. Richter, N. Nishioka and T. Deutsch, "Ultraviolet laser-induced fluorescence of colonic tissue: basic biology and diagnostic potential," Lasers in Surgery & Medicine, **12**, 63-78 (1992).
11. T. D.Wang, JM. Crawford, M.S. Feld, Y. Wang, I. Itzkan, J. Van Dam, "In vivo identification of colonic dysplasia using fluorescence endoscopic imaging," Gastrointestinal Endoscopy, **49**(4 Pt 1), 447-55 (1999).
12. M.A. Mycek, K.T. Schomacker, N.S. Nishioka, "Colonic polyp differentiation using time-resolved autofluorescence spectroscopy," Gastrointestinal Endoscopy **48**, 390-4 (1998).
13. A. Zuluaga, U. Utzinger, A. Durkin, H. Fuchs, A. Gillenwater, R. Jacob, B. Kemp, J. Fan, R. Richards-Kortum, "Fluorescence EEMs of Human Tissue: A System for in vivo Measurements and Method of Data Analysis," Applied Spectroscopy **53**, 302-310 (1999).
14. R.A. Zangaro, L. Silveira, R. Manoharan, G. Zonios, I. Itzkan, R. Dasari, J.C. Van Dam, M.S. Feld, "Rapid multiexcitation fluorescence spectroscopy system for in vivo tissue diagnosis," Applied Optics **35**, 5211-5219, (1996).
15. J.A. Zuclich, T. Shimada, T.R. Loree, I. Bigio, K. Strobl, Shuming Nie, "Rapid noninvasive optical characterization of the human lens," Lasers in the Life Sciences, **6**, 39-53 (1994).
16. I.M. Warner, G.D. Christian, E.R. Davidson, J.B. Callis, "Analysis of multicomponent fluorescence data," Analytical Chemistry **49**, 564-573 (1977).
17. J.C. Zenklusen, S.L. Stockman, S.M. Fischer, C.J. Conti, I.B. Gimenez-Conti, "Transforming growth factor-beta 1 expression in Syrian hamster cheek pouch carcinogenesis," Molecular Carcinogenesis **9**, 10-16 (1994).
18. I.B. Gimenez-Conti, D.M. Shin, A.B. Bianchi, D.R. Roop, W.K. Hong, C.J. Conti, T.J. Slaga, "Changes in keratin expression during 7, 12-dimethylbenz[α]anthracene-induced hamster cheek pouch carcinogenesis," Cancer Res **50**, 4441-4445 (1990).
19. J.K. Dhingra, X. Zahng, K. McMillan, S. Kabani, R. Manoharan, I. Itzkan, M.S. Feld, S.M. Sharpshay, "Diagnosis of head and neck precancerous lesions in an animal model using fluorescence spectroscopy," Laryngoscope **108**, 471-475 (1998).
20. J.K. Dhingra, D.F. Perrault, K. McMillan, E.E. Rebeiz, S. Kabani, R. Manoharan, I. Itzkan, M.S. Feld, S.M. Shapshay, "Early diagnosis of upper aerodigestive tract cancer by autofluorescence," Arch Otolaryngol Head Neck Surg **122**, 1181-1186 (1996).
21. C.T. Chen, H.K. Chiang, S.N. Chow, C.Y. Wang, Y.S. Lee, J.C. Tsai, C.P. Chiang, "Autofluorescence in normal and malignant human oral tissues and in DMBA-induced hamster buccal pouch carcinogenesis," Journal of Oral Pathology & Medicine **27**, 470-474 (1998).
22. D.L. Heintzelman, U. Utzinger, H. Fuchs, A. Zuluaga, K. Gossage, A.M. Gillenwater, R. Jacob, B. Kemp, R. Richards-Kortum, "Optimal Excitation Wavelengths for In Vivo Detection of Oral Neoplasia Using Fluorescence Spectroscopy," Photochemistry and Photobiology, in press (2000).
23. L. Coghlan, U. Utzinger, R. Richards-Kortum, C. Brookner, A. Zuluaga, I. Gimenez-Conti, M. Follen, "Fluorescence Spectroscopy of Epithelial Tissue Throughout the Dysplasia-Carcinoma Sequence in an Animal Model: Spectroscopic Changes Precede Morphologic Changes," Lasers in Surgery and Medicine submitted (2000).
24. W.R. Dillon, M. Goldstein, *Multivariate Analysis Methods and Applications*, (John Wiley & Sons, 1984), Chap. 10.
25. B. Chance, "Optical Method," Annu. Rev. Biophys. Biophys. Chem. **20**, 1-28 (1991).

1. Introduction:

Many clinical studies have shown that fluorescence spectroscopy offers promise for *in vivo* detection of epithelial dysplasia [1-3], in organ sites such as the oral cavity [4-7], the cervix [8, 9], and the colon [10-12]. In most of these studies, tissue fluorescence is measured at several excitation wavelengths prior to biopsy and then correlated with histologic diagnosis. It is well known that the choice of excitation and emission wavelength determines which tissue chromophores contribute to the resulting spectrum and strongly affects the shape and intensity of fluorescence spectra [1, 2]. However, a limitation of most previous clinical studies of fluorescence spectroscopy is that the choice of excitation wavelength has not been fully optimized.

Recently, several systems have been developed which enable measurement of fluorescence emission spectra at many excitation wavelengths rapidly *in vivo* [13-15]. These

#26869 - $15.00 US Received October 20, 2000; Revised December 01, 2000

spectra can then be assembled into a fluorescence excitation emission matrix (EEM), which fully characterizes the fluorescence properties of a multi-chromophore sample [16]. In this study, we report the use of such a system to measure fluorescence EEMs *in vivo* from epithelial tissue throughout the dysplasia-carcinoma sequence using a model of chemically driven carcinogenesis in the Syrian hamster cheek pouch; EEMs were analyzed to determine which excitation wavelengths yield optimal diagnostic ability for neoplasia.

The hamster cheek pouch carcinogenesis model, using chronic treatments with the carcinogen dimethylbenz[α]anthracene (DMBA) in the cheek pouch, is well characterized [17, 18]. Histologically, the 16-week treatment protocol pushes the epithelial lining of the cheek pouch through stages of inflammation, hyperplasia, dysplasia, and both benign and malignant tumor formation. Epithelial hyperplasia develops after only a few treatments with DMBA. Dysplastic lesions, resembling human premalignant lesions, are seen after 6-8 weeks of treatment. After about 10 weeks, papillomas and carcinomas begin to appear [17].

Several *in vivo* studies have been performed in which carcinoma was initiated with DMBA and then tissue fluorescence spectra were measured [18-20]. Dhingra [19] measured fluorescence emission spectra *in vivo* from DMBA induced precancers and early cancers in the hamster cheek pouch. Neoplastic lesions showed characteristic fluorescence between 630-640 nm emission at 410 nm excitation. Using this as a diagnostic criterion, 45 of 49 lesions were correctly diagnosed. Similar results were obtained in fluorescence measurements of early cancers of the oral cavity in a small clinical trial [20]. Chen [21] investigated 330 nm excited fluorescence emission spectra from DMBA induced lesions in the hamster cheek pouch and noted that the emission intensity at 380 nm decreased in neoplastic tissues while that fluorescence intensity at 460 nm increased and shifted to 470 nm in neoplastic tissues. Similar spectral profiles were observed in human oral malignant and normal tissues [21]. These studies suggest that fluorescence measurements from the hamster cheek pouch model of carcinogenesis can yield insight into the spectroscopic changes that accompany the development of neoplasia in humans.

The goal of the study described in this paper was to characterize the fluorescence emission spectra of non-neoplastic and neoplastic epithelium in this model at a large number of excitation wavelengths and to use these data to determine the fluorescence excitation/emission wavelength combinations which contain the most diagnostic information for the detection of neoplasia. We measured fluorescence EEMs at 18 excitation wavelengths ranging from 330-500 nm and fluorescence emission wavelengths from 340 to 700 nm from 371 sites in 20 control and 42 DMBA treated animals. We applied a method to analyze fluorescence EEMs to determine which excitation and emission wavelengths contain the most diagnostic information and to estimate the expected performance of diagnostic algorithms based on this information [22]. In this study, we found that the combination of full emission spectra from three excitation wavelengths (360 nm, 370 nm and 420 nm excitation) resulted in a sensitivity of 90% and specificity of 95%. These excitation wavelengths compare favorably to those found to be optimal for detection of neoplasia in human subjects [22].

2. Methods

2.1 Animal treatment protocol

This study consisted of 62 Syrian hamsters in two arms; 42 animals were treated with the carcinogen 0.5% DMBA in mineral oil to induce gradual epithelial carcinogenesis, and 20 control animals were treated only with mineral oil. Animals were initially treated three times per week; however, after two weeks, treatments were reduced to twice per week, and the concentration of DMBA was reduced to 0.25% due to significant erosion and exudative reaction in the DMBA group. In each case, the treatment substance was applied to the deepest recess of the right cheek pouch with a No. 5 camel hair brush. On a weekly basis, at least one animal from each arm was sacrificed and the cheek pouch was surgically removed

#26869 - $15.00 US Received October 20, 2000; Revised December 01, 2000

for histologic analysis. This protocol was approved by the Animal Care Use Committee at The University of Texas M.D. Anderson Cancer Center and was conducted at the Department of Carcinogenesis campus, an Association for the Assessment and Accreditation of Laboratory Animal Care International accredited facility, in accordance with the *Guide for the Care and Use of Laboratory Animals.* Table 1 summarizes the study design.

2.2 DMBA fluorescence

Experiments were performed to determine whether the fluorescence from DMBA affects *in vivo* fluorescence measurements of the hamster cheek pouch; results showed that no residual DMBA fluorescence could be detected in the fluorescence spectra measured from tissue at 48 hours following DMBA application [23]. The DMBA treatment days were scheduled to ensure that the fluorescence measurements always took place at least 48 hours after the DMBA treatment.

2.3 Hamster fluorescence measurements

The fluorescence of the control and DMBA treated hamster cheek pouches was measured weekly. The spectroscopic system used to measure fluorescence excitation-emission matrices (FastEEM) has been described in detail previously [13]. Briefly, the system measures fluorescence emission spectra at 18 excitation wavelengths, ranging from 330 nm to 500 nm in 10 nm increments with a spectral resolution of 7 nm. The system incorporates a fiberoptic probe, a Xenon arc lamp coupled to a monochromator to provide excitation light and a polychromator and thermo-electrically cooled CCD camera to record fluorescence intensity as a function of emission wavelength (Figure 1). Fluorescence excitation power at 400 nm was approximately 90 μW distributed over a spot of 2 mm diameter. Each week, fluorescence spectra were measured from a pre-selected group of animals. Approximately 10 minutes prior to measurements, animals were anesthetized with 50 mg/kg ketamine HCl (Fort Dodge, Overland Park, KS 66210) delivered intraperitoneally. At time of measurement the hamsters ranged in weight from 100 to 160 grams. The hamster cheek pouch was manually everted with a gloved index finger of the handler to expose the deepest recess of the pouch. The hamster was placed in a lateral recumbent position within the handler's gloved hand. Before fluorescence spectra were measured, the pouch was rinsed with saline solution. The fluorescence measurement process took approximately 2-3 minutes.

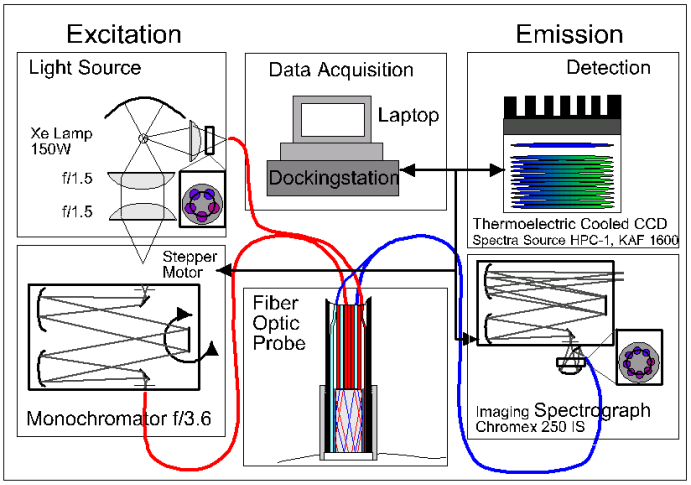

Fig. 1. Block diagram of system used to measure fluorescence EEMs.

As a negative control a background EEM was obtained with the probe immersed in a non-fluorescent bottle filled with distilled water at the beginning of each measurement day. Then a fluorescence EEM was measured with the probe placed on the surface of a quartz

#26869 - $15.00 US Received October 20, 2000; Revised December 01, 2000

cuvette containing a solution of Rhodamine 610 (Exciton, Dayton, OH) dissolved in ethylene glycol (2 mg/mL) at the beginning of each measurement day.

To correct for the non-uniform spectral response of the detection system, the spectra of two calibrated sources were measured at the beginning of the study; in the visible an NIST traceable calibrated tungsten ribbon filament lamp was used and in the UV a deuterium lamp was used (550C and 45D, Optronic Laboratories Inc, Orlando, FL). Correction factors were derived from these spectra. Dark current subtracted EEMs from animals were then corrected for the non-uniform spectral response of the detection system. Variations in the intensity of the fluorescence excitation light source were corrected using a calibrated photodiode (818-UV, Newport Research Corp.). Finally, corrected fluorescence intensities from each site were divided by the fluorescence emission intensity of the Rhodamine standard at 460 nm excitation, 580 nm emission. Thus, data illustrated in this paper are not the absolute fluorescence intensities of tissue but rather given in calibrated intensity units relative to the Rhodamine standard. This calibration method corrects for day to day variations in instrument throughput. Following each day of measurements, the probe was disinfected using Metricide (Metrex Research Corp.). Measurements were made from the control group first, to prevent transmission of residual DMBA to these animals.

2.4 Histological evaluation

Excised hamster cheek pouches and biopsy samples were fixed with formalin, sectioned and stained with hematoxylin and eosin for histological evaluation. Slides were reviewed by two investigators (L.C., I.G.-C.), blinded to the spectroscopic results. Samples were classified into 9 categories based on the most severe histopathologic finding: normal, inflammation, ulceration, hyperplasia, dysplasia (grades I-III), carcinoma in situ (CIS), and squamous cell carcinoma (SCC). Table 1 contains the final histopathologic diagnoses. 74 total sites were reviewed histopathologically; diagnoses were concordant in 66 sites and discordant in 8. Data from the 8 sites with discordant diagnoses were discarded. These samples are noted in Table 1.

#26869 - $15.00 US Received October 20, 2000; Revised December 01, 2000

Table 1: Study design for the DMBA treated and control group animals. Colored boxes indicate measurement events. Histopathologic diagnoses are shown with abbreviations, where N=normal, INF=inflammation, U=ulceration, H=hyperplasia, I=grade I dysplasia, II=grade II dysplasia, III=grade III dysplasia, CIS=carcinoma in situ, and SCC=squamous cell carcinoma. Discrepant diagnoses are indicated with D. Yellow shaded boxes indicate those non-neoplastic measurements used in algorithm development; orange shaded boxes indicate those neoplastic measurements used in algorithm development; pink shaded boxes indicate those measurements with fluorescence EEMs discarded during data review. Light blue shaded boxes indicate measurement where diagnosis was undetermined and therefore not used for algorithm development.

Animal #	Week																
DMBA	1	2	3	4	5	6	7	8	9	10	11	12	13	14	15	16	17
1	N																
2	H																
3			U														
4			D														
5					D												
6					D												
7							I										
8							I										
9									II								
10									D								
11											CIS						
12											CIS						
13													II				
14													D				
15											I						
16															D		
17																	CIS
18																	SCC
19																	SCC
20																	SCC
21																	SCC
22		U															
23		INF															
24				D													
25				D													
26						II											
27						II											
28								II									
29										II							SCC
30										II							
31										III							
32												III					
33												III					
34														II			
35														CIS			
36														III			
37										III						SCC	
38										II							SCC
39										D							
40								CIS			III						
41								III						CIS			
42								II	III								

#26869 - $15.00 US
Received October 20, 2000; Revised December 01, 2000

Control	1	2	3	4	5	6	7	8	9	10	11	12	13	14	15	16	17
43			N														
44					N												
45							N										
46									N								
47																	INF
48													INF				
49															N		
50																	N
51											H						
52																	N
53				N													
54																	
55								N									
56										H							
57										N			INF				
58										H						N	
59										H							N
60								N			INF						
61								N						N			
62								N									N

2.5 Data Review

EEMs were measured from 371 total sites. All spectra were reviewed by a single investigator blinded to the pathologic results (DLH). Spectra were discarded if EEM files were not saved properly due to software error, instrument error, operator error, probe movement, and the presence of room light artifacts at wavelengths in at least one of the emission spectra. Spectra from a total of 44 sites were discarded in this process.

2.6 Data analysis

EEMs were examined visually by 6 investigators (U.U., R.D, D.L.H, A.Z., C.B, R.R.K.) to note differences in data from non-neoplastic and neoplastic samples. Figure 2 shows a typical example of an EEM from a non-neoplastic and a high grade neoplastic area. An advantage of this animal model is that it allows one to monitor the spectroscopic changes which take place throughout the dysplasia to cancer sequence; Figure 3 shows a video which illustrates fluorescence EEMs from a single hamster throughout the 17 week DMBA treatment regime. Each EEM was normalized to unity at 390 nm excitation, 460 nm emission. This hamster was biopsied at week 10 and sacrificed at week 17. At baseline, the hamster cheek pouch was normal, at week 10 the biopsy showed grade II dysplasia and at week 17, the histology showed a squamous cell carcinoma.

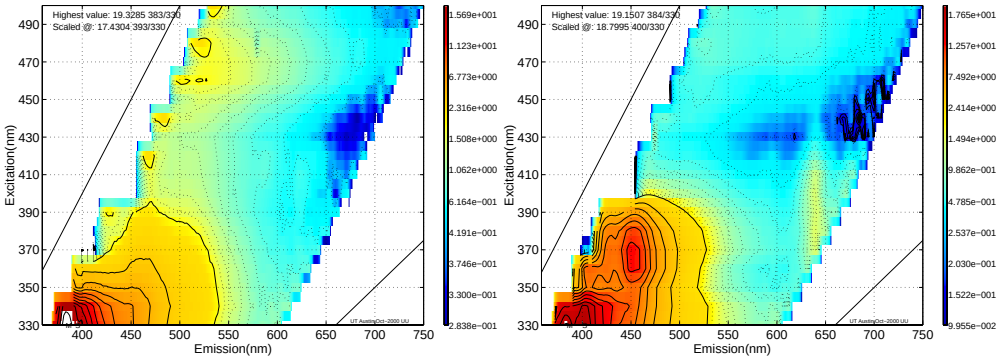

Fig. 2. Fluorescence EEMs of (left) non-neoplastic and (right) neoplastic hamster cheek pouch.

#26869 - $15.00 US Received October 20, 2000; Revised December 01, 2000

Fluorescence data in the data set were analyzed to determine which excitation and emission wavelengths contained the most diagnostically useful information and to estimate the performance of diagnostic algorithms based on this information [22]. We considered algorithms based on multi-variate discriminant analysis. We developed algorithms based on combinations of emission spectra at various excitation wavelengths in order to determine which excitation wavelengths contained the most diagnostic information. The algorithm development process, consisted of the following major steps: (1) data pre-processing to reduce inter-animal variations, (2) data reduction using principal component analysis to reduce the dimensionality of the data set, and (3) feature selection and classification to develop algorithms which maximized diagnostic performance and minimized the likelihood of over-training. For the purpose of the algorithm development and evaluation, the data were classified into one of two classes: non-neoplastic (normal, inflammation, ulceration, hyperplasia) and neoplastic (all grades of dysplasia, CIS and SCC). If histopathology indicated a site was non-neoplastic, then all measurements preceding that date were assumed to be non-neoplastic. If histopathology indicated a site was neoplastic, then all measurements after that date were assumed to have neoplasia.

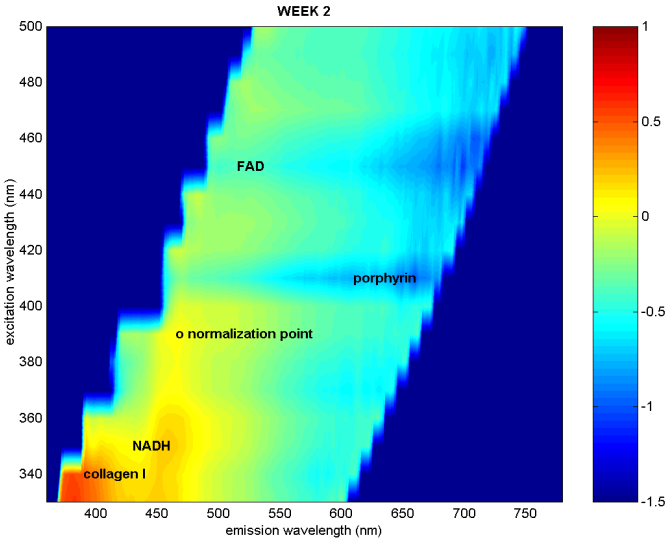

Fig. 3. Video illustrating fluorescence EEMs each week for a hamster treated with DMBA. Biopsy at week 10 showed grade II dysplasia and histology at week 17 showed squamous cell carcinoma (1.459 KB).

Our previous work illustrates that spectra of oral cavity in humans obtained *in vivo* show large patient to patient variations in intensity that can be greater than the inter-category differences [22]. Therefore, we explored pre-processing methods to reduce the inter-animal variations, while preserving inter-category differences; here, we normalized in two fashions. In the first method, all emission spectra in a concatenated vector were normalized by the largest emission intensity contained within that vector. In the second method, all emission spectra were normalized to their individual intensity maximum.

In this study, fluorescence emission spectra were measured at 18 different excitation wavelengths. One goal of the data analysis was to determine which combination of excitation wavelengths contained the most diagnostic information. Combinations of emission spectra from up to three excitation wavelengths were considered. Limiting the device to three wavelengths allows for construction of a reasonably cost-effective clinical spectroscopy system. Here, we evaluated the diagnostic performance of all possible selections of up to three wavelengths chosen from the 18 possible excitation wavelengths. For each of the 987

#26869 - $15.00 US Received October 20, 2000; Revised December 01, 2000

combinations of one to three excitation wavelengths, spectra from the entire data set were used to develop multi-variate algorithms to separate non-neoplastic and neoplastic tissues based on their fluorescence emission spectra at all possible wavelength combinations. Principal component analysis was performed using the entire dataset and eigenvectors accounting for 65% and 95% of the total variance were retained. Principal component scores associated with these eigenvectors were calculated for each sample. Discriminant functions were then formed to classify each sample as non-neoplastic or neoplastic. The classification was based on the Mahalanobis distance, which is a multivariate measure of the separation of a point from the mean of a dataset in n-dimensional space [24]. The sample was classified to the group from which it has the shortest Mahalanobis distance. The sensitivity and specificity of the algorithm were then evaluated relative to diagnoses based on histopathology. Overall diagnostic performance was evaluated as the sum of the sensitivity and the specificity, thus minimizing the number of misclassifications (when prevalence of disease and non-disease are approximately equal). The performance of the diagnostic algorithm depended on the principal component scores that were included. From the available pool of principle component scores, the single principal component score yielding the best initial performance was identified, and then the principal component score that most improved this performance was selected. This process was repeated until performance was no longer improved by the addition of principal components scores, or all available scores were selected. Then, for the top 25 choices, we redeveloped and evaluated algorithm performance using cross-validation and re-ranked performance to guard against over-training. Table 2 provides the best performing combinations of one to three excitation wavelengths. For the top performing combinations of three excitation wavelengths, histograms depicting the frequency of occurrence of each excitation wavelength were plotted (Figure 4).

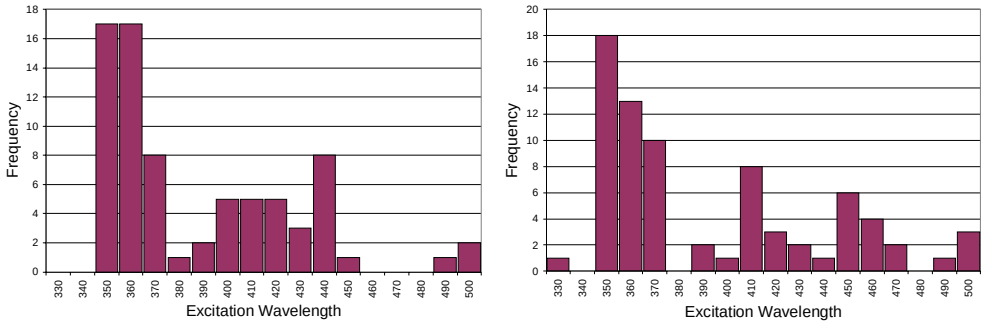

(a) (b)

Fig. 4. Histograms depicting the frequency of occurrence of each excitation wavelength in the 25 top performing combinations of 3 excitation wavelengths under cross-validation using (a) normalization method 1 and (b) normalization method 2.

3. Results

EEMs were measured from 371 total sites. Data from 132 non-neoplastic sites and 31 neoplastic sites were available for algorithm development and evaluation (Table 1). Figure 2 shows a typical EEM of a non-neoplastic site and a site with high grade neoplasia. The EEM of the neoplastic site shows increased fluorescence near 360-370 nm excitation and 450 nm emission. This spectral region corresponds to emission from NADH and collagen cross-links. The EEM of the neoplastic site also shows decreased fluorescence near 460-470 nm excitation and 530 nm emission. This spectral region corresponds to FAD fluorescence as well as collagen cross-links. The EEM of the neoplastic sample shows increased fluorescence at 410 nm excitation, 630 nm emission, corresponding to porphyrin emission. Additionally, the

#26869 - $15.00 US Received October 20, 2000; Revised December 01, 2000

EEM of the neoplastic site shows deeper valleys near 420 nm excitation and emission, corresponding to hemoglobin absorption.

Table 2: Algorithm results for top performing combinations of 1, 2 and 3 excitation wavelengths (λ_{ex}) using cross validation and both normalization methods.

# λ_{ex}	Norm. Method	% Variance	λ_{ex}	Sensitivity $\#_{samples} = 31$	Specificity $\#_{samples} = 132$
1	1	65%	360	87.1%	94.7%
1	1	95%	360	93.5%	92.4%
1	2	65%	360	87.1%	94.7%
1	2	95%	360	93.5%	92.4%
2	1	65%	360, 370	93.5%	90.2%
2	1	95%	360, 390	87.1%	97.7%
2	2	65%	350, 410	87.1%	98.5%
2	2	95%	360, 390	90.3%	95.5%
3	1	65%	360, 370, 420	90.3%	94.7%
3	1	95%	360, 370, 380	90.3%	97.7%
3	2	65%	360, 450, 460	90.3%	93.9%
3	2	95%	330, 350, 410	93.5%	93.9%

Figure 3 shows a video of fluorescence EEMs from each week for a hamster treated with DMBA. The aforementioned spectral changes are seen in sequential fashion in this video, with fluorescence increasing near 360 nm and 410 nm excitation, decreasing near 460 nm excitation and absorption increasing at 420 nm. This animal was biopsied at week 10, and showed grade II dysplasia. Histology at week 17 showed squamous cell carcinoma.

Table 2 shows the algorithm results for top performing combinations of 1, 2 and 3 excitation wavelengths using cross validation. Sensitivities and specificities achieved are close to and exceed 90%. The two normalization methods used produced similar results. When eigenvectors accounting for either 65% or 95% of the total variance in the data were used, similar sensitivities and specificities were achieved, indicating that the good algorithm performance is not based on random fluctuations due to noise in the data. As the number of excitation wavelengths was increased from one to three, both sensitivity and specificity increased slightly.

Figure 4 show histograms depicting the frequency of occurrence of each excitation wavelength in the 25 top performing combinations of 3 excitation wavelengths under cross-validation. Using both normalization methods, excitation wavelengths near 350-370 nm contain the most diagnostically useful information. Using normalization method 1 (Figure 4a), excitation wavelengths from 400-440 nm also appear to be diagnostically useful; whereas for normalization methods 2 (Figure 4b) 410 and 450 nm excitation appear to be diagnostically useful. These excitation wavelength ranges correspond well to those in Table 2.

4. Discussion and Conclusions:

The hamster cheek pouch carcinogenesis model, using chronic treatments of DMBA, provides a well controlled system in which to investigate the changes in fluorescence which occur in squamous epithelial tissue throughout carcinogenesis. This model has broad applications to human cancers including, but not limited to, the oral cavity, the lung and esophagus, the

#26869 - $15.00 US Received October 20, 2000; Revised December 01, 2000

uterine cervix, vagina, vulva and skin. Thus, this animal model can be used to investigate many emerging optical technologies for detection of neoplasia and dysplasia.

In this paper, we examined the changes in autofluorescence throughout carcinogenesis. Results showed increased fluorescence near 350-370 nm excitation and decreased fluorescence near 450-470 nm excitation with neoplasia. These changes are consistent with the expected increase in NADH fluorescence and decrease in FAD fluorescence with neoplasia [25]. Furthermore, results show increased porphyrin fluorescence and increased hemoglobin absorption throughout the development of squamous cell carcinoma. An important advantage of this animal model relative to studies in human subjects is that one can ethically observe these spectroscopic changes as dysplasias progress to invasive cancers.

Using this model system, algorithms for detection of dysplasia and neoplasia using one to three excitation wavelengths yield both high sensitivity and specificity. With three excitation wavelengths sensitivity and specificity exceed 90% - results which would be acceptable clinically and superior to many commonly used screening and diagnostic techniques. The optimal diagnostic excitation wavelengths identified using this model - 350-370 nm excitation and 400-450 nm excitation - are quite similar to those identified in a similar study [22] involving oral cavity neoplasia in human subjects - 350, 380 and 400 nm excitation. Thus, in the case of fluorescence spectroscopy, results from this animal model can guide the development of techniques to detect dysplasia in humans. This model should be explored further in the development of new optical diagnostic technologies.

Acknowledgments:

We gratefully acknowledge Donna Schutz, Pam Kille, and Dale Weiss for assistance with in vivo procedures, Jimi Lynn Rosborough-Brandon for histological services and Holger Fuchs for assistance in acquiring data. This work was funded in part by Physician Referral Service Research Support Grant 4-0021080 and by the NIH (CA16672).